Quaternary Geochronology 94 (2026) 101746

Contents lists available at ScienceDirect

Quaternary Geochronology

journal homepage: www.elsevier.com/locate/quageo

Novel rock luminescence dating of snow petrel stomach-oil deposits from East Antarctica

Rachel K. Smedley [a,*], David Small [b], Erin L. McClymont [b], Michael J. Bentley [b], Dominic A. Hodgson [c], Alice Graham [b]

[a] Department of Geography and Planning, University of Liverpool, Liverpool, UK
[b] Department of Geography, Durham University, Durham, UK
[c] British Antarctic Survey, Cambridge, UK

ARTICLE INFO

Keywords:
Palaeoclimate
Antarctica
Luminescence
Snow petrels

ABSTRACT

The discovery of long-term accumulations of snow petrel stomach-oil deposits in Antarctica have provided an excellent opportunity to reconstruct changes in climate, ice-sheet thickness and sea ice. However, providing age constraints on the deposition of these biological accumulations can be challenging, particularly when they extend beyond the radiocarbon age limit (ca. 55 ka). Luminescence dating is successfully used here to provide accurate ages for rocks underlying and incorporated into snow petrel stomach-oil deposits in East Antarctica. The agreement between the different luminescence signals measured from K-feldspars, in addition to the independent age control (radiocarbon dating) gives confidence in the results. We show the potential for reconstructing ice-sheet histories from multiple burial events with prior exposure durations recorded in the luminescence depth profiles of the rocks. Our study extends beyond the traditional sedimentary contexts usually used for luminescence dating, and into biological accumulations, which has not previously been done. We show that rock luminescence dating can overcome some challenges of using radiocarbon dating for biological accumulations (e.g. young carbon contamination, marine reservoir uncertainty) and can potentially extend the dateable age range to at least Marine Isotope Stage 5 according to the saturation limit of the luminescence signal measured for these samples. This is key for using these stomach-oil deposits to quantify the contribution to sea-level rise provided by Antarctic Ice Sheet retreat, and changes in sea ice during the last warm interglacial period experienced on Earth.

1. Introduction

Novel palaeoclimate archives can provide important information on past environmental change in places where traditional records (e.g., lakes and peat bogs) are scarce. Antarctica is one such location where, due to persistent cold and low biological activity, continuous records of past environmental change have primarily been restricted to continental ice cores, offshore marine sediments, and lacustrine sediments at the ice sheet margins (e.g., Delmonte et al., 2002; Verleyen et al., 2011; Mulvaney et al., 2012). Recently, accumulations of stratified stomach-oil deposits, regurgitated by snow petrels (*Pagodroma nivea*) at their nest sites, have been used to reconstruct past changes in sea-ice distribution and climate around Antarctica based on the intrinsic links between the deposits and sea-ice conditions within the birds' foraging range (e.g., Berg et al., 2019; McClymont et al., 2022a; Stevenson et al., 2025). The accumulation of the deposits has also been used to track ice-sheet thinning histories based on nest availability at different altitudes (Hiller et al., 1988), and the changing distribution of breeding colonies across the last glacial cycle (McClymont et al., subm.). Beyond Antarctica, other biological accumulations including animal and hominin middens (e.g., McCarthy et al., 1996; Zazula et al., 2007; Chase et al., 2009, 2012; Wurz et al., 2022) have provided insights into environmental change on timescales from the Holocene to (at least) Marine Isotope Stage (MIS) 5.

Obtaining accurate age constraints for all palaeoenvironmental records is vital for interpreting them within a wider regional and global context. Radiocarbon dating has been widely applied where there is sufficient organic content. However, it has some challenges. For example, bioturbation can introduce a disturbed stratigraphy and age reversals (e.g., Robins and Robins, 2011), while post-depositional microbial activity can potentially introduce contaminating "young carbon"; this has been reported for some snow petrel stomach-oil deposits

* Corresponding author.
E-mail address: rachel.smedley@liverpool.ac.uk (R.K. Smedley).

https://doi.org/10.1016/j.quageo.2026.101746
Received 28 January 2026; Received in revised form 17 March 2026; Accepted 23 April 2026
Available online 30 April 2026

(Penny, 2025). Additionally, radiocarbon dating of snow petrel stomach-oils can only provide minimum age constraints for the onset of accumulation. Specifically for snow petrel stomach-oil deposits in Antarctica, there is also uncertainty introduced into ages by a variable marine reservoir correction resulting from changes in sea ice extent through time (McCarthy et al., 1996; Heaton et al., 2023). Finally, some snow petrel stomach-oil records which are of great interest extend beyond the limit of the radiocarbon method, so additional methods are needed (Penny, 2025). Luminescence dating of rock surfaces covered by or incorporated into biological accumulations offers a new opportunity to constrain the ages of deposition and accumulation. Here, we provide the first burial ages from rocks incorporated into snow petrel stomach-oil deposits from East Antarctica.

2. Rock surface luminescence dating

Luminescence dating can determine the time that has elapsed since a mineral grain (typically quartz of K-feldspar) was last exposed to sunlight (bleached) and subsequently buried (see Murray et al., 2021; Smedley, 2018). Recent developments using luminescence depth profiles recovered from surfaces of crystalline rocks have extended the versatility of the luminescence technique, which now includes both burial dating (e.g., Jenkins et al., 2018; Freiesleben et al., 2015) and exposure dating (e.g., Laskaris and Liritzis, 2011; Sohbati et al., 2011; Lehmann et al., 2018). For this approach, luminescence profiles are measured with depth into a rock surface. They extend from luminescence signals representing the last exposure event in the upper portion of the rock, down to the saturated luminescence signals measured at depth, which have never been exposed to sunlight. Where the luminescence signal of quartz is dim due to short sediment transport pathways or particular bedrock lithologies (e.g., Antarctica), the infra-red stimulated luminescence (IRSL) signals of K-feldspar is preferred as a robust and (usually) brighter alternative to the optically stimulated luminescence signal of quartz (e.g., Theilen et al., 2023); this is even more important for dating of rocks which are not sensitised to the same extent as sand- or silt-sized grains during their recycling in the natural environment.

Luminescence dating of K-feldspar can be performed using different stimulation temperatures (e.g., 50, 150 and 225 °C), where the higher temperatures are considered more reliable (Thomsen et al., 2008) as they circumvent the anomalous fading phenomenon (Wintle, 1973). Since the introduction of the new rock luminescence techniques, most studies (e.g., Freiesleben et al., 2015; Lehmann et al., 2018; Ageby et al., 2022) have only utilised the lower temperature (IR_{50}) signal as it bleaches more efficiently with depth into rock surfaces compared to higher-temperature IRSL signals (e.g., Luo et al., 2018; Ou et al., 2018). However, previous studies have shown that the IRSL signals measured at different temperatures have different luminescence characteristics (e.g., bleaching rates, fading rates, saturation levels) that can be exploited during measurements (e.g., Smedley et al., 2021; Elkadi et al., 2022). Here, we apply a multiple elevated temperature (MET; Li and Li, 2011) protocol using stimulation temperatures of 50, 150 and 225 °C. If the ages determined with all three signals are in agreement, it evidences the reliability of the data in comparison to examples where the ages diverge.

There are several advantages of rock luminescence dating that make it particularly useful for dating biological accumulations (e.g., snow petrel stomach-oil deposits): (i) quartz and/or K-feldspar is found almost ubiquitously in rocks providing dateable material in most settings; (ii) any rock surface that has been exposed to sunlight and subsequently covered (i.e., by ice, sediment or organic accumulation) can be dated; and (iii) the dose-rate used for dating is dominated by the rocks internal dose-rate with a much smaller contribution from the surrounding material; thus, uncertainty introduced by the matrix heterogeneity and variable water content will be minimal in comparison to dating sand- and silt-sized grains. As such, rock luminescence dating provides an excellent opportunity to constrain the initiation of organic accumulations, such as bird stomach-oil deposits in Antarctica.

3. Methods

3.1. Sample collection and preparation

Six rocks were collected from five snow petrel stomach-oil deposits for luminescence dating. These samples come from four sites in Dronning Maud Land, and one in Coats Land, East Antarctica (Fig. 1, Table 1): Reichelnevet (samples R1 and R2; deposit 2612MUM1; Fig. 2) and Torsviktoppen (T1; 0101MUM6) in the Heimefrontfjella, and Utsteinen Nunatak (U1 and U2; UTMUM003 and UTMUM011, respectively) in the Sør Rondane Mountains and Marø Cliffs (M1; 1401MUM2) located within the Theron Mountains in Coats Land. All sites and samples are shown in Fig. S1. The stomach-oil deposits were collected during daylight, but the uppermost surfaces of the sampled rocks were protected from sunlight exposure by the covering of stomach-oil, which is naturally opaque. Furthermore, studies have shown that the luminescence signal of rocks sampled in white light conditions were not compromised for dating (e.g., Ou et al., 2018). The stomach-oil deposits were kept frozen (−20 °C) until sampling. Rocks were extracted in the lab under subdued red-light conditions from the base of the deposit or from within the deposit. Rock cores (7 mm diameter) were extracted from the upper surfaces of the rocks using an Axminster bench-top, pillar drill equipped with a water-cooled, diamond-tipped drill bit. Care was taken to avoid locations close to previously cut faces or outer edges of the deposit to minimise potential for bleaching of the rock surface. The rock cores were generally quite short (6 – 17 mm) due to the small size of the sampled rocks. Where possible, replicate cores were taken, however, due to the small size of the rocks available, the number of cores varied per sample. Each core was subsequently sliced at a thickness of ~0.7 mm using a Buehler IsoMet low-speed saw equipped with a water-cooled, 0.3 mm diameter diamond-tipped wafer blade. Slices were then mounted in stainless steel cups for luminescence measurements.

3.2. Luminescence measurements

3.2.1. Palaeodose

All luminescence measurements were performed on a Risø TL/OSL reader (TL-DA-15) with a $^{90}Sr/^{90}Y$ beta irradiation source. IRSL signals were detected in blue wavelengths using a photo-multiplier tube fitted with Schott BG-39 (2 mm thickness) and Corning 7-59 (2 mm thickness) filters. A MET-post-IR IRSL sequence was used to determine IRSL signals at three different temperatures (50, 150 and 225 °C) simultaneously (IR_{50}, $pIRIR_{150}$ and $pIRIR_{225}$ signals, respectively). After heating at 1 °C/s, the rock slices were held at the stimulation temperature (i.e. 50, 150 and 225 °C) for 60 s to ensure all the disc was at temperature prior to IR stimulation (Jenkins et al., 2018; Elkadi et al., 2021). Luminescence depth profiles were determined for each core by measuring the natural signal (L_n) normalised using the signal measured in response to a 52 Gy test-dose (T_n), hereafter termed the L_n/T_n signal (Fig. S2). The luminescence signal was determined by subtracting the background signal (final 20 s, 40 channels) from the initial signal (0 – 3.5 s, 7 channels). A large test-dose (52 Gy) was used to reduce the impact of thermal transfer/incomplete resetting of the IRSL signal between measurements (after Liu et al., 2016). The slices were accepted if they passed the following screening criteria (accounting for the associated uncertainties): (1) the test dose response was 3 s above the background, (2) the test-dose uncertainty was less than 10%, (3) recycling ratios were within the range of ratios 0.9 to 1.1, and (4) recuperation was less than 5 % of the response from the largest regenerative dose. D_e values were subsequently calculated from the slices passing all the screening criteria.

Rock slices from sample R1 were used for dose-recovery experiments after a 7 h bleach in a Hoenle UVACUBE 400. A 35 Gy given dose was administered to three discs with zero doses administered to a further three discs to determine a residual D_e value after artificial bleaching. The artificially-bleached residual D_e values were subtracted from the recovered dose to determine the dose-recovery ratio. The rock slices

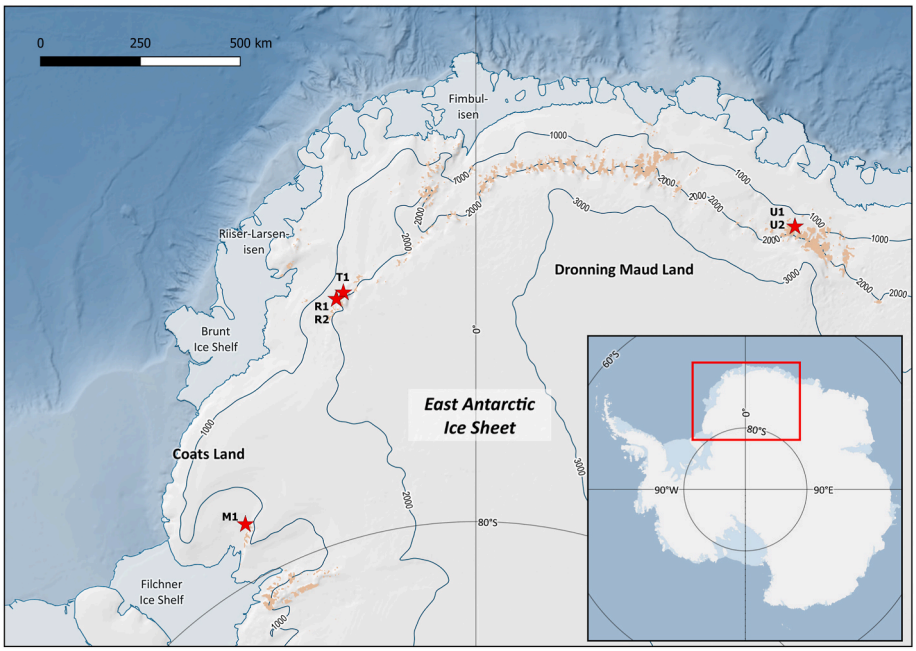

Fig. 1. Location map of stomach-oil deposits collected from East Antarctica (red stars) with rock sample codes shown. Inset shows location within Antarctica.

Table 1
Sample information for rocks collected for luminescence analysis from the snow petrel stomach oil deposits. The radiocarbon ages for each deposit (for full details see Table S1) are shown alongside the age results using the three luminescence signals in this study.

Deposit	Lab code	Site	Latitude (DD)	Longitude (DD)	Altitude above ice (m)	Rock dimensions (mm)	Lithology	Basal radiocarbon age (cal. Ka BP)	Fading-corrected IR_{50} age (ka)	$pIRIR_{150}$ age (ka)	$pIRIR_{225}$ ages (ka)
2612MUM1	R1	Reichelnevet	−74.7067	−11.8081	55	73 × 35 x 25	Gneiss	7.1 ± 0.3	2.4 ± 0.4	5.5 ± 0.6	6.6 ± 0.5
2612MUM1	R2	Reichelnevet	−74.7067	−11.8081	55	78 × 35 x 34	Gneiss	7.1 ± 0.3	4.7 ± 1.7	6.2 ± 0.6	7.6 ± 0.9
0101MUM6	T1	Torsviktoppen	−74.5950	−11.1249	11	38 × 20 x 16	Gneiss	2.5 ± 0.2	5.3 ± 2.7	8.6 ± 5.1	8.7 ± 3.6
1401MUM2	M1	Marø Cliffs	−78.7969	−27.5572	354	40 × 38 x 25	Dolerite	0.5 ± 0.2	6.0 ± 1.9	26.2 ± 4.6	35.9 ± 6.7
UTMUM003	U1	Utsteinen	−71.9629	23.3345	20	60 × 28 x 28	Granite	1.1 ± 0.2	-	-	-
UTMUM011	U2	Utsteinen	−71.9636	23.3396	6	34 × 28 x 20	Granite	26.6 ± 3.8[a]	-	-	-

[a] Radiocarbon age was taken from the top of the deposit for this sample.

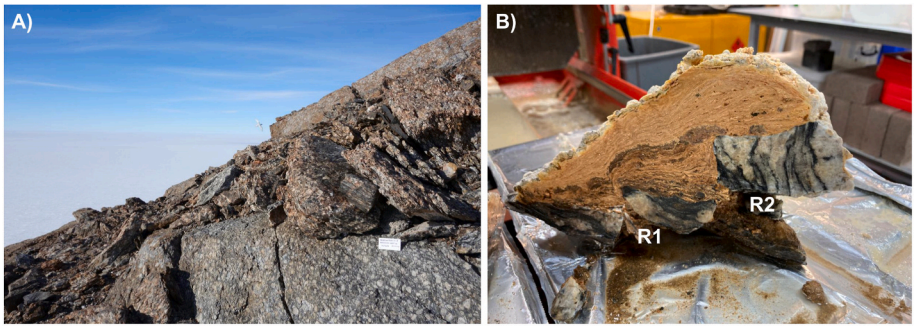

Fig. 2. Photographs showing: (A) the depositional context of an example site at Reichelnevet with the white (ca. 14 × 8 cm) sign marking the location of the stomach-oil deposit at the opening of a rock cavity nest site; and (B) the extracted snow petrel stomach-oil deposit with sampled rocks (R1 and R2) incorporated. A snow petrel can be seen in flight in the middle of panel A for scale.

successfully recovered the given dose (considering the ±1 σ uncertainties) to within 10 % using the IR_{50} (0.84 ± 0.07) and $pIRIR_{225}$ (0.85 ± 0.05). However, it recovered the given dose within ±20 % using the $pIRIR_{150}$ (0.80 ± 0.04) signal. The luminescence signal intensities were bright for this sample (see Fig. S2A) so unlikely to have been related to weak signal intensities. Alternatively, the slight deviation in the recovered dose using the $pIRIR_{150}$ signal was likely caused by the fact that the residual dose subtracted from the recovered dose was not measured on exactly the same slices; thus, the residual dose measured could have slightly overestimated the true residual doses that were incorporated into the slices used to recover the given dose. Fading rates (*g*-values, Aitken, 1985) were determined for each rock sample and normalised to two days (Huntley and Lamothe, 2001). The weighted means and standard errors of the *g*-values for all discs were 5.7 ± 0.6

%/decade (IR_{50} signal), 0.0 ± 0.7 %/decade ($pIRIR_{150}$ signal) and −0.8 ± 0.8 %/decade ($pIRIR_{225}$ signal) (Table S2); thus, only ages determined using the IR_{50} signal required correction for sample-specific fading rates.

3.2.2. Environmental dose-rates

Due to the depositional context of the sampled rocks, the determination of the environmental dose-rate was complex. Each rock was positioned on top of lithologically similar bedrock and directly overlain by the snow petrel stomach-oil deposit (e.g., Fig. 2). To calculate the environmental dose-rate throughout burial for each sample, U, Th and K concentrations were measured for each individual rock sample using inductively coupled plasma mass spectrometry (Table S3). Given the biological nature of the deposit, we assume zero concentrations of U and Th. However, K can be sourced through foraging by the birds, and so the K concentration for the matrix overlying the rocks (i.e. the stomach-oil) was measured using portable x-ray fluorescence (pXRF). K concentrations of 0.3 % (2612MUM1B) and 0.5 % (UTMUM011) were measured and so an average of the two samples was used for dose-rate calculations (0.4 ± 0.1 %) for all samples. Sensitivity tests were also performed varying the K concentration of the overlying matrix (i.e. stomach-oil deposits) from 0 to 3 % to assess the impact on the environmental dose-rate.

Cosmic dose-rates were calculated after Prescott and Hutton (1994). Given the aridity of the depositional environment, we assumed 0 % water contents for both the stomach-oil deposit and the rock itself (after Jenkins et al., 2018). The average down-core grainsize of K-feldspar in each sample was measured from ten randomly selected grains per slice using *ImageJ* and used for dose-rate calculations (Table S3). The grainsizes measured in this study were smaller than previous studies (e.g., Ageby et al., 2022; Jenkins et al., 2018) and so the internal dose-rates calculated will be lower. The grainsizes of K-feldspar within rocks are dictated by the composition of the rocks and their formation conditions (e.g. temperatures, rate of cooling or crystallisation) (Deer et al., 2013), which can account for the difference in grainsizes to previous studies. The mean grain size for the stomach-oil deposits surrounding the rock was assumed to be 2 μm. An internal K-content of 10 ± 2 % (Smedley et al., 2012) and internal U and Th concentrations of 0.3 ± 0.1 ppm and 1.7 ± 0.4 ppm (Smedley and Pearce, 2016) were used to determine the internal alpha and beta dose-rates of the rocks. An a-value of 0.10 ± 0.02 (Balescu and Lamothe, 1993) was used to calculate the alpha dose-rates for the rocks. As the gamma field was not homogeneous for 30 cm surrounding each sample, the gamma dose was scaled according to Aitken (1985) based on the rock thickness, density of the bird stomach-oil (1.5 g cm^{-3}), gneiss (2.75 g cm^{-3}) and/or dolerite (3.00 g cm^{-3}), water content (assumed to be 0 %) and U, Th and K concentrations of the rock and the overlying bird stomach-oil (Table 1). The gamma dose-rate was also modelled to include the contributions from the underlying rock, which was the same composition as the sampled rock, and the air above the bird stomach-oil. Finally, the variation of the dose-rate with depth into each cobble surface was determined (after Freiesleben et al., 2015; Riedesel and Autzen, 2020) and used to calculate depth-specific burial ages.

3.2.3. Calculation of burial ages

The D_e values determined for each rock slice from the cores of each sample was divided by the modelled depth-specific dose-rate to determine down-core ages. Jenkins et al. (2018) calculate burial ages by combining the ages for all slices on an inferred plateau using a simple average. However, (i) this approach does not account for age uncertainties on each rock slice; (ii) it does not consider that any scatter could be incorporated into the inferred well-bleached plateau from additional sources beyond the counting statistics (e.g., intrinsic luminescence characteristics); and (iii) the inferred plateau is not determined via statistical means, rather an arbitrary line drawn through the data, which is difficult to decide upon when considering the age uncertainties. Here, we prefer to consider that all the rock slices for each sample are equivalent to partially-bleached distributions, which contain a well-bleached population (similar to D_e distributions measured from sand). This is appropriate as the age-depth profile for the rock cores extend from the interior shielded from sunlight exposure (with no bleaching of the luminescence signal), through the bleaching front (with partial bleaching of the luminescence signal) and to the surface which was exposed to sunlight (likely a well bleached luminescence signal). As such, we determine ages for each age distribution using the minimum age model (MAM). By applying the MAM to the ages determined for all of the slices for each sample we can: (i) incorporate the uncertainty on each age estimate into the sample age calculation; (ii) incorporate additional scatter (σ_b) into the well-bleached age distribution caused by sources beyond the counting statistics (e.g., intrinsic luminescence characteristics); and (iii) statistically identify the ages that form the well-bleached portion of the partially-bleached distribution. A σ_b of 0.10 was used to determine the MAM ages based on the overdispersion value determined from the dose-recovery experiments.

3.2.4. Rock opacity

After luminescence measurements were performed, each rock slice was analysed to investigate potential changes in rock composition with depth. Down-core red-green-blue (RGB) values were determined for each sample to investigate whether there was any colour variation within the sample, and externally between samples; thus, providing a semi-quantitative tool to detect variability in rock opacity (Meyer et al., 2018). Raster images of RGB were obtained for each rock slice using an EPSON Expression 11000XL flatbed scanner at 1200 dpi resolution. Mean and standard deviations of the RGB values for each rock slice were calculated using the *raster* package in R (version 2.9-23; Hijmans, 2019).

3.3. Independent age control from radiocarbon

Radiocarbon ages for the snow petrel stomach-oil deposits were measured as part of NERC (NE/K003674/1) and ANTSIE (ERC Reference 864,637) projects (McClymont et al., subm.; Table 1). Where available, we include relevant bracketing ages (top and bottom) for the samples used for rock luminescence dating (Table S1). Radiocarbon ages were calibrated following McClymont et al. (2022b) using the MARINE20 calibration curve (Heaton et al., 2020) and a ΔR of 670 ± 50 years derived from penguin bones at Hope Bay (cf. Björck et al., 1991). This marine reservoir correction represents Holocene conditions with generally low sea-ice abundance (after Heaton, 2021; Heaton et al., 2023). We consider this appropriate as all (but one) radiocarbon date are Holocene in age. The exception (sample 62,290 from the top of the UTMUM011 deposit) gives an apparent age from the Last Glacial Maximum when sea-ice extent would have been greater, which would need a larger ΔR correction (Heaton et al., 2023). However, we do not present a corresponding luminescence burial age for the UTMUM011 deposit (constrained by sample U2) and so any assumption about the ΔR correction does not impact the comparison of ages from the two approaches.

4. Results

4.1. Environmental dose-rate variability

Quantifying the K concentration of the stomach-oils overlying the rocks used for luminescence burial dating was challenging as it may have varied between sites (although not considerably as the birds will have maintained a broadly similar diet through time). pXRF measurements show little difference between the K concentrations of deposits 2612MUM1B from the Reichelnevet site (0.3 %) and UTMUM011 from the Utsteinen site (0.5 %). Furthermore, we performed sensitivity tests where the K concentration of the overlying matrix was varied from 0 to 3 % to assess the impact on the environmental dose-rates. The results show that even a large increase from 0 to 3 % K for the stomach-oil had a very

small impact upon the environmental dose-rates when modelled with depth into the rock surface (Fig. S3A–D). The surface slices would have been impacted to the largest extent by variation in the stomach-oil K concentration but only measured a small difference for samples R1 (3 %), T1 (13 %), M1 (12 %) and R2 (6 %) when varying the K from 0 to 3 % (Fig. S3E). Consequently, it is unlikely that variability in the K concentration of the bird stomach-oil would have had an impact on the ages beyond the uncertainties already incorporated into dating as the majority of the dose-rate is provided by the rock itself where we have measured U, Th and K concentrations for all samples. Therefore, it was appropriate to assume a K concentration of 0.4 ± 0.1 % for the stomach-oil deposits overlying all the samples in this study.

4.2. Sample characteristics

The rock slices used for all samples were dark in colour, but varied

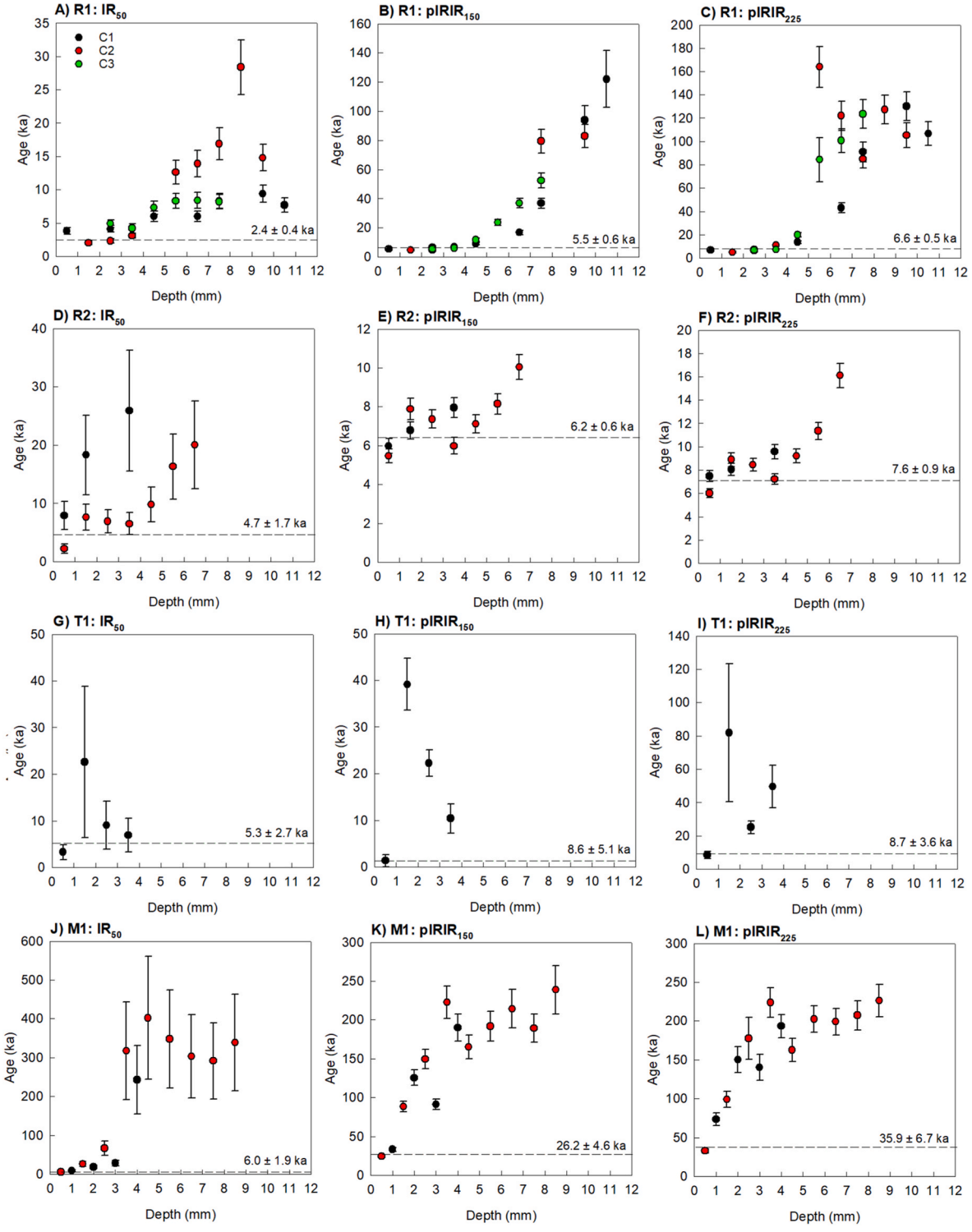

Fig. 3. Luminescence depth plots for the samples in this study measured using the IR_{50} (fading corrected), $pIRIR_{150}$ and $pIRIR_{225}$ signals from K-feldspar. Data are plotted for each individual core (C) measured. The dashed line shows the sample age.

between samples, especially for samples T1 and R2, which were both gneiss (Fig. S4; Fig. S5). The luminescence signal intensity of rock slices can be highly variable, especially across the different IRSL signals, where the IR_{50} signal is typically brighter than the $pIRIR_{150}$, which is in turn brighter than the $pIRIR_{225}$ signal. To be able to determine D_e values for a rock slice, we need to detect a measurable luminescence signal. The luminescence signals for all samples were measurable across the IR_{50}, $pIRIR_{150}$ and $pIRIR_{225}$ signals (Fig. S2). However, the IRSL signals for sample T1 were significantly dimmer than the rest of the samples (Fig. S2C). This likely translated into poor precision of the ages determined.

4.3. Extent of luminescence signal resetting

To determine an accurate burial age, each sample must have been ice free and exposed to sunlight prior to burial for a sufficient amount of time to fully reset (or bleach) the luminescence signals used for dating (i.e. the IR_{50}, $pIRIR_{150}$ and/or $pIRIR_{225}$ signals). Broadly speaking, the longer the sunlight exposure time prior to burial, the deeper the bleaching front propagates into the rock surface. Rock slices that were bleached prior to burial will form a plateau in apparent burial ages (i.e., L_n/T_n values or normalised luminescence) in the upper portion of the core. The depth of this plateau will be dictated by the prior exposure time, in addition to the light attenuation properties of each rock (e.g., the rock opacity). Four samples (R1, T1, M1 and R2) determined a luminescence depth profile indicative of light penetration into the rock surface during prior exposure to sunlight (Fig. 3), while two samples (U1 and U2) did not (Fig. 4).

The luminescence depth profile for sample R1 suggests that this rock experienced sufficient sunlight exposure prior to burial as the burial ages are broadly consistent up to 4 mm depth across three replicate cores for the IR_{50}, $pIRIR_{150}$ and $pIRIR_{225}$ signals (Fig. 3A–C). For sample R2 (from the same deposit), the large uncertainties on the fading-corrected IR_{50} ages for Core 1 make it difficult to assess plateau extent (Fig. 3D). However, Core 2 has a lower age at the surface (up to 1 mm) followed by a plateau up to 4 mm, which was also observed in both the $pIRIR_{150}$ (Fig. 3E) and $pIRIR_{225}$ (Fig. 3F) signals. Luminescence depth profiles with 'steps' in its plateau can be indicative of multiple burial events (e.g., Freiesleben et al., 2015; Jenkins et al., 2018). Sample T1 produced ages with large uncertainties and scatter in the luminescence depth profiles (Fig. 3G–I), which is likely to be related to the low signal-intensities measured for this sample (Fig. S2C). However, the lowest age in the profile was measured at the surface slice for all three IRSL signals, suggesting the potential that this sample was reset at the surface. Finally, sample M1 displays a plateau up to ~2 mm depths for the IR_{50} signal and up to 1 mm depths for the $pIRIR_{150}$ signal (two discs), and then only the surface slice (Fig. 3J–L) was suggestive of some signal resetting for the $pIRIR_{225}$ signal. The presence of a small plateau in both the IR_{50} and $pIRIR_{150}$ signals suggests that this sample may have been exposed to some sunlight prior to burial to fully reset these signals. However, as only the surface slice is potentially reset in the $pIRIR_{225}$ signal, it is difficult to assess the extent of bleaching prior to burial; thus, the $pIRIR_{225}$ signal is not considered for dating of this sample.

Two samples (U1 and U2) did not measure luminescence depth profiles and so could not have been exposed to sufficient sunlight prior to burial to reset the luminescence signal (Fig. 4). Consequently, D_e values and ages were not determined for samples U1 and U2. These samples were taken from the same site (Utsteinen nunatak; Fig. 2) and so it is possible that the lack of sunlight exposure relates to site specific conditions such as slope aspect and/or shade produced by nearby obstructions or being deposited within a rock cavity (see Fig. S1 D and E).

4.4. Burial ages

Ages were determined using the D_e values measured with the IR_{50} (fading-corrected), $pIRIR_{150}$ and $pIRIR_{225}$ signals (Figs. 3 and 5). The

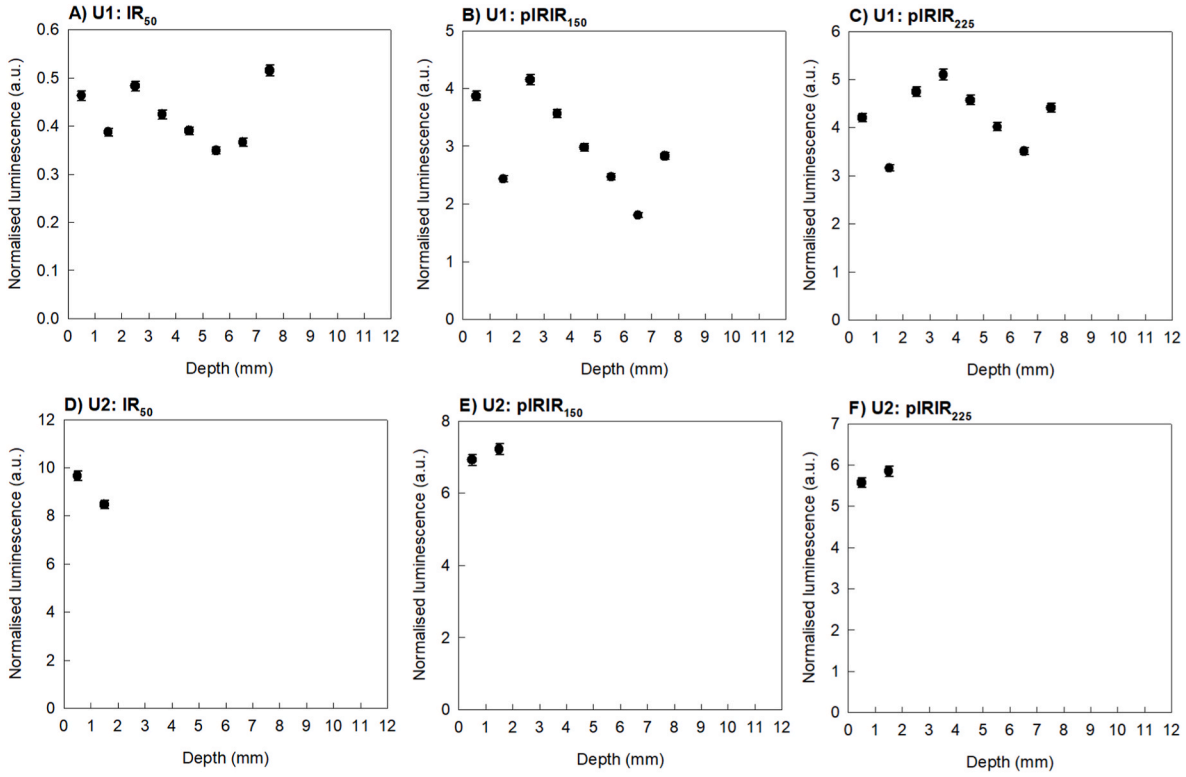

Fig. 4. Luminescence depth plots measured using the IR_{50}, $pIRIR_{150}$ and $pIRIR_{225}$ signals from K-feldspar for the samples in this study where the profiles did not suggest bleaching prior to burial. Data are plotted for the one core measured for each sample. Only normalised luminescence (L_n/T_n) values are shown for samples U1 and U2 as they did not show evidence of sunlight exposure prior to burial.

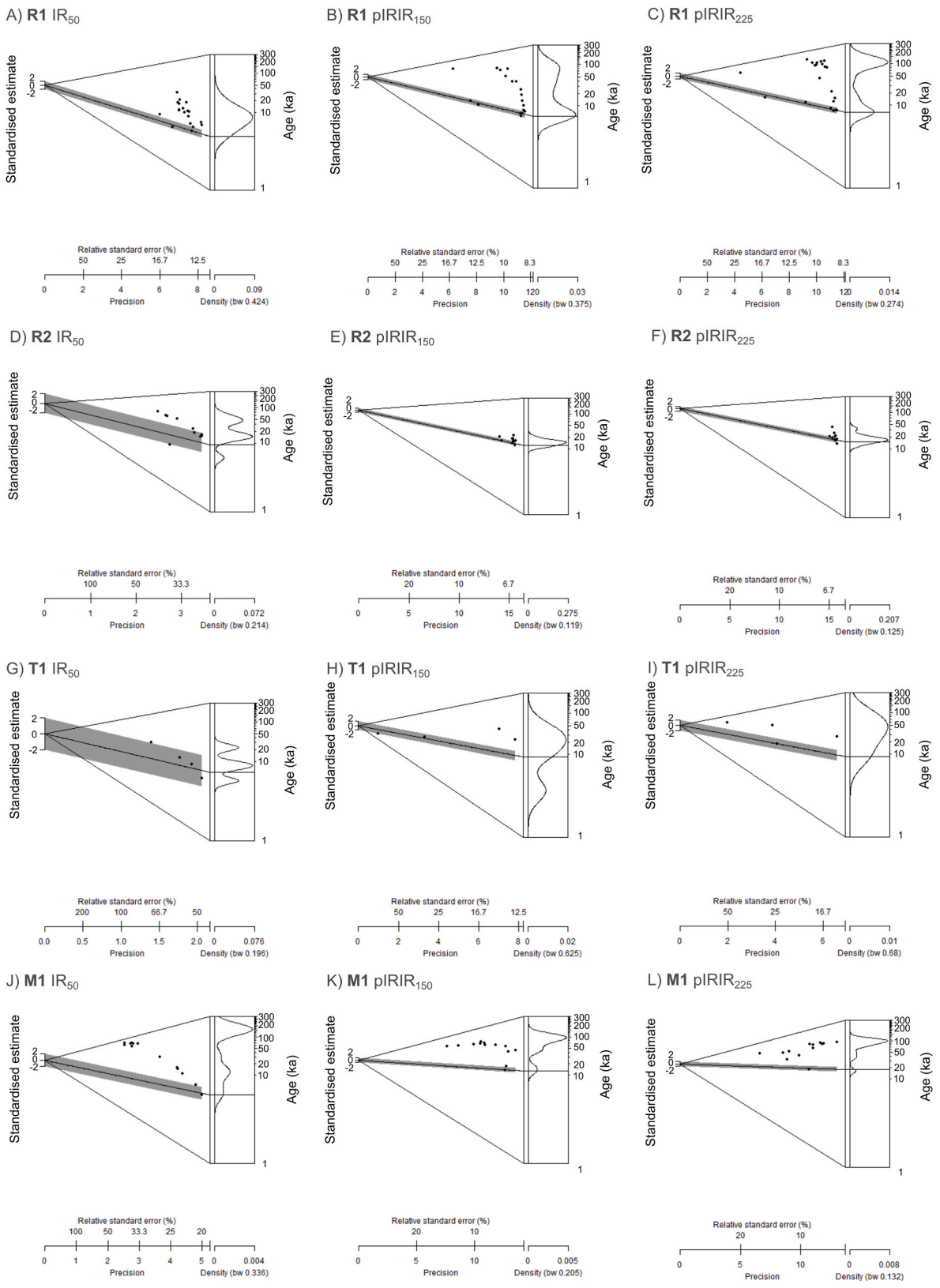

Fig. 5. Abanico plots showing the ages determined for rock slices of samples R1, R2, M1 and T1. The grey shading shows the MAM ages determined for each dataset using a σ_b of 0.10.

luminescence depth profiles of both samples (R1 and R2) from Reichelnevet are characterised by a plateau and are considered to have been well-bleached prior to burial. The luminescence ages for these samples are broadly comparable across all IRSL signals (IR_{50}: 2.4 ± 0.4 ka and 4.7 ± 1.7 ka; $pIRIR_{150}$: 5.5 ± 0.6 ka and 6.2 ± 0.6 ka; $pIRIR_{225}$: 6.6 ± 0.5 ka and 7.6 ± 0.9 ka). We note that for sample R1, the IR_{50} age (2.4 ± 0.4 ka) is lower than both the $pIRIR_{150}$ (5.5 ± 0.6 ka) and $pIRIR_{225}$ (6.6 ± 0.6 ka) ages from the same sample, in addition to the IR_{50} age from sample R2 (4.7 ± 1.7 ka). Nevertheless, the pIRIR ages for both samples agree within uncertainties and they are all consistent with independent age control provided by the basal radiocarbon age (SUERC-42052) of 7.1 ± 0.3 cal Ka BP from the bottom of the stomach-oil deposit (Table 1).

The steps in the luminescence depth profile of sample R2 from Reichelnevet showed potential evidence for multiple burial cycles being recorded by the rock. To calculate ages for these potential burial cycles, the finite mixture model (FMM) was used to identify the presence of three age components within the age distribution. The two main (younger) components in the age distribution for sample R2 were 6.1 ± 0.8 ka (33 % of the population) and 7.5 ± 0.8 ka (57 % of the population). The ages determined for the different components were broadly comparable but slightly older for the $pIRIR_{225}$ signal at 7.0 ± 1.3 ka (26 % of population) and 9.0 ± 0.9 ka (63 % of the population). The ages of the oldest components for each signal were not useful as they were taken from across the bleaching front of the luminescence depth profile, which was not fully reset prior to burial.

At the Torsviktoppen site, the lack of an obvious plateau for sample T1 highlights lower confidence in the reliability of the ages determined for this sample as we cannot be certain that it was exposed to sufficient sunlight prior to burial. Nevertheless, the IR_{50} (5.3 ± 2.7 ka), $pIRIR_{150}$ (8.6 ± 5.1 ka) and $pIRIR_{225}$ (8.7 ± 3.6 ka) ages calculated for the surface slice of T1 are all in agreement within ± 1σ uncertainties, and are also in (very) broad agreement with a basal radiocarbon age of 2.5 ± 0.2 ka cal. BP), which provides a minimum age for the onset of biogenic accumulation. However, we note that this agreement is reliant upon the large uncertainties on the apparent burial ages caused by the low signal intensities measured for this sample.

For sample M1 from the Marø cliffs, there was a large discrepancy between the ages calculated for the fading-corrected IR_{50} signal (6.0 ± 1.9 ka) and the $pIRIR_{150}$ signal (26.2 ± 4.6 ka). The $pIRIR_{225}$ signal did not show a plateau and so no age was calculated. The large discrepancy between the IR_{50} and $pIRIR_{150}$ ages and limited plateau recorded for the $pIRIR_{150}$ signal would suggest that this sample experienced limited sunlight exposure prior to burial; thus, bleaching prior to burial was limited. In such cases, the fading-corrected IR_{50} signal is more likely to produce an accurate burial age as it resets faster in response to sunlight. However, it is difficult to assess the accuracy of the burial ages for sample M1 as the age inversion between the top (1.0 ± 0.2 ka) and basal (0.5 ± 0.2 ka) radiocarbon ages questions the reliability of the independent age control. The fading-corrected IR_{50} age (6.0 ± 1.9 ka) is interestingly similar to the age of the stomach-oil deposits at Reichelnevet (~7 ka).

In summation, samples R1 and R2 from Reichelnevet produced luminescence burial ages that are consistent within and between samples (especially for the pIRIR ages) and which are consistent with independent age control provided by radiocarbon dating. Sample T1 from Torsviktoppen also produces burial ages consistent with independent age control but these ages are characterised by large uncertainties. The reliability of the ages for sample M1 from the Marø cliffs is questioned due to limited bleaching prior to burial but is similar to those from Reichelnevet (~7 ka).

5. Discussion

5.1. Successful dating of biological accumulations

The ages determined for the Reichelnevet site (samples R1 and R2) are in good agreement with the radiocarbon age from the bottom of the stomach-oil deposit (Table 1). Together the ages suggest that the stomach-oil deposition began ~7 ka, which is consistent with the timing of regional deglaciation (Grieman et al., 2024; Suganuma et al., 2022) resulting in ice-free conditions at the nest site. Although the luminescence depth profiles for sample T1 from Torsviktoppen did not show obvious evidence of a significant plateau suggestive of extensive bleaching, the luminescence ages obtained from the surface slice were also in broad agreement with the available radiocarbon chronology when accounting for the large uncertainties caused by low signal intensities. These samples show the success of using rock luminescence dating to constrain the timing of stomach-oil deposition. Given the elevated position of the nesting sites at Reichelnevet (55 m) above the present ice surface (Table 1), it is unlikely that ice fluctuations would have covered this site since the rocks were deposited and so would not have affected the luminescence depth profiles measured. In contrast, the nesting site at Torsviktoppen was only 11 m above the present ice surface (Table 1) and so there is greater potential for the sunlight exposure to have been restricted to this sample by fluctuating ice volume prior to its burial. The three other samples in this study were less successful in providing age constraints, but for different reasons.

The lack of any luminescence depth profile (i.e. bleaching) in samples from Utsteinen (samples U1 and U2) is notable given that previous studies demonstrate that luminescence depth profiles can develop within periods as short as days (e.g., Smedley et al., 2021; Ou et al., 2018; Freiesleben et al., 2023). However, the dark colour of samples U1 and U2 (Fig. S4) implies that these rocks have high opacity and so light would be attenuated more rapidly in these samples in comparison to previous studies that used lithologies with lower rock opacity (e.g., sandstone, granites and quartzite). Ou et al. (2018) have shown that the luminescence depth profiles of a dark greywacke sample remained very shallow relative to other lithologies despite their controlled bleaching experiments extending up to the equivalent of 91 days of daylight exposure in the UK. Furthermore, sunlight intensity in Antarctica can be much reduced due to the angle of sunlight being more oblique compared with lower latitudes, particularly in unfavourable (e.g. south facing) aspects (e.g., Fuhrmann et al., 2022) or where there are significant obstructions on the skyline (e.g., being located within a cavity or shielded by boulders and mountain peaks). Furthermore, the nesting sites at Utsteinen were only 6 m (U1) and 20 m (U2) above the present ice surface (Table 1) and so are more likely to have been covered by small-scale fluctuations in ice volume. Finally, the transport pathways of the rocks prior to incorporation within the deposit are potentially very short (e.g., merely falling off the cavity roof) and there may be limited opportunity for some exposure to sunlight before burial; this was likely the case for sample M1. Considering all these factors, it is not surprising that some rocks did not contain any evidence of a luminescence depth profile indicative of signal resetting prior to burial.

For sample T1 from Torsviktoppen, the sunlight exposure event prior to burial was not sufficiently long to reset the luminescence signal to depths much beyond the surface slice (up to 1-2 mm). This poses challenges as it is difficult to show that the luminescence signal of a single (surface) slice was well bleached prior to burial. However, it has previously been applied in Antarctica to reconstruct sea-levels using fine-grained volcanic rocks and some granites (Simms et al., 2011). In such cases, consistency in derived burial ages across the IR_{50}, $pIRIR_{150}$ and $pIRIR_{225}$ signals for K-feldspar can increase confidence that a sample was well-bleached prior to burial (after Murray et al., 2012). Similarly, a lack of consistency between the IR_{50}, $pIRIR_{150}$ and $pIRIR_{225}$ ages decreases confidence that the samples were well-bleached prior to burial. Given that the IR_{50} signal bleaches faster than the $pIRIR_{150}$ and $pIRIR_{225}$ signals in response to sunlight (e.g., Smedley et al., 2015; Colarossi et al., 2015), the IR_{50} signal would be better reset in scenarios with minimal sunlight exposure (e.g. sample T1) prior to burial than the pIRIR signals. However, there are also factors that can cause underestimation of the IR_{50} signal relative to the pIRIR signals. In this study, fading rates

measured for the IR_{50} signal were high (up to 8.7 ± 1.0 %/decade) and all samples required a fading correction (Huntley and Lamothe, 2001) to determine ages. This fading correction produced significant uncertainty in the IR_{50} ages and is reliant upon an ability to accurately measure fading rates. Furthermore, there is increased potential for the IR_{50} signal to be contaminated by emissions from Na-feldspar compared to the pIRIR signals (Thomsen et al., 2018). Ages (unknowingly) determined from Na-feldspar could potentially cause age underestimation as the environmental dose-rate calculations assume the luminescence signal used for dating is emitted solely by K-feldspar with higher internal K-contents of 10 ± 2 % (after Smedley et al., 2012).

Overall, we show that rock luminescence dating can be successful in determining accurate ages in the challenging context of dating rocks under and within the biological accumulations of snow petrel stomach-oil deposits. The variable levels of bleaching observed likely relates to variable sunlight exposure conditioned by specific sample and site factors, some of which (but not all) can be mitigated prior to sampling. Therefore, the best approach is to sample a larger population of rocks and consider the individual site characteristics such as aspect, shading and history of ice-sheet cover (i.e. height above present ice; Table 1) when interpreting ages. It is encouraging that four samples from a total of six rocks that we opportunistically obtained from our snow petrel stomach-oil deposits showed evidence of bleaching. This suggests that a significant proportion of rocks within biological deposits may be suitable for rock luminescence dating, especially if a more focussed and strategic sampling strategy is employed. Furthermore, it is likely that the rock luminescence dating approach may be even more successful for biological accumulations at lower latitudes than Antarctica where there is improved exposure due to the angle of sunlight being less oblique.

5.2. *Future opportunities*

The depth of the well-bleached plateau in the luminescence depth profiles can reveal information about the length of time each rock was exposed to sunlight prior to burial, which is beneficial in the absence of cosmogenic nuclide ages. Well-bleached plateaus that extend to deeper depths (e.g. R1; Fig. 3A–C) imply longer sunlight exposure periods prior to burial, while shallower profiles are suggestive of shorter sunlight exposure periods prior to burial (e.g. M1; Fig. 3J and K). Previous studies have provided models that can determine the age of the prior exposure in buried rocks (Freiesleben et al., 2015). More complete luminescence depth profiles that fully capture the saturation portion of the profile at lower depths into the rock are required to apply these exposure dating models accurately. None of the luminescence depth profiles measured for samples in this study are sufficiently complete to calculate prior exposure ages using the approach of Freiesleben et al. (2015) due to the small size of the rocks and the preferred nest habitat within the cavities of the snow petrels. However, given that all the samples have similar rock opacity (Fig. S5), we can infer relative sunlight exposure histories prior to burial. Rock samples R1 and R2 were evidently exposed to sunlight for the longest period prior to burial being 55 m above the present ice sheet surface, while samples T1 (11 m above ice) and M1 (354 m above ice) were exposed for less time, but more than samples U1 and U2 (20 m and 9 m above ice) that did not have any evidence of sunlight exposure prior to burial.

Multiple burial events have previously been reported from rock luminescence burial dating (e.g., Freiesleben et al., 2015; Jenkins et al., 2018) and are evidenced by 'stepped' luminescence depth profiles. Although it must be acknowledged that some variability in age may be introduced by variability in K concentrations with depth (Ou et al., 2022). Sample R2 from the Reichelnevet site shows some evidence of a 'step' in the luminescence depth profile across the IR_{50}, $pIRIR_{150}$ and $pIRIR_{225}$ signals (Fig. 3D–F). When the finite mixture model (FMM) is fitted to the age distribution of sample R2 using the $pIRIR_{150}$ signal (Fig. S6), it identifies three components in the age distribution at 6.1 ± 0.8 ka (33% of the population) and 7.5 ± 0.8 ka (57 % of the population) and 9.6 ± 2.0 ka (10 %). Note that the oldest component here is not an accurate age but averaging across the slices that form the bleaching front (i.e., not fully reset prior to burial). While acknowledging that this interpretation is tentative, it is possible that multiple burial events can be recorded within samples such as those presented here. This could potentially reflect fluctuations of the ice margin over the site, a scenario that is more likely for samples closer to the present ice surface. Alternatively, given the situation of each sample within a cavity at each nest site, it is most likely that any hiatuses reflect episodic transport of the clast with intermittent shielding/burial (e.g., by snow) prior to incorporation within the deposit. For our samples, the oldest 'step' in the luminescence depth profile would provide a minimum constraint on ice-free conditions (i.e. sunlight exposure) at the rock surface. For sample R2, this suggests ice-free conditions at 7.5 ± 0.8 ka, which is in agreement with a regional deglaciation estimate (Grieman et al., 2024; Suganuma et al., 2022). Similarly, there is potential for other rock surfaces in Antarctica that are presently shielded from sunlight (e.g. by glacier ice) to record prior burial events that can be related to the broader ice-sheet history (e.g., Balco et al., 2023; Small et al., 2025).

Finally, rock luminescence dating can extend the dateable age range beyond the limits of radiocarbon dating (ca. 55 ka cal. BP; Hajdas et al., 2021). While most of the deposits investigated here date from the Holocene, deposits that return infinite radiocarbon ages have also been reported (e.g., Penny, 2025). As these old deposits cannot currently be dated, we cannot place them within any regional or global palaeoenvironmental context. It is possible that they were deposited during the Last Interglacial (i.e. MIS5), which would have important implications for interpreting ice-sheet extent (and therefore sea-level rise), and changing sea-ice conditions at that time. If basal (or near basal) rocks can be recovered from biological accumulations from the snow petrel (or any other organism), then rock luminescence dating can likely provide accurate ages as the limit of luminescence burial dating of K-feldspar can exceed >125 ka (e.g., Table S4; Buylaert et al., 2012). However, this is dependent on the magnitude of the environmental dose-rate (i.e., lower dose-rates facilitate older ages) and the luminescence properties of the individual rocks (i.e., their saturation limits; Table S4).

6. Conclusions

Luminescence dating of rocks buried within accumulations of snow petrel stomach-oils in East Antarctica provided ages in agreement with independent age control (radiocarbon dating). Variable levels of signal resetting were observed between samples, which likely relates to variable sunlight exposure experienced prior to burial conditioned by specific sample and site factors. Comparing the different luminescence signals of K-feldspar (IR_{50}, $pIRIR_{150}$ and $pIRIR_{225}$) allowed us to assess whether the signal resetting prior to burial was sufficient to derive accurate ages with confidence. This showed that three of the samples were sufficiently exposed to sunlight prior to burial (Reichelnevet, Marø Cliffs), two samples were not exposed at all (Utsteinen), and one sample (Torsviktoppen) was exposed but only the lower temperature (IR_{50}) IRSL signal was sufficiently reset for dating. We observed variable durations of prior sunlight exposure before burial that could potentially be linked to the length of time spent ice free prior to nest occupation or post-depositional re-mobilisation of the rock in the nest site. Our samples also highlight the potential for multiple burial events to be preserved in the luminescence depth profiles of rocks that could provide insights into past fluctuations in the ice sheet. Applying rock luminescence dating in this novel context has shown that we can extend chronological control beyond traditional sedimentary contexts constrained by previous studies and into dating biological accumulations, which has not previously been done. Furthermore, the saturation limits of the luminescence signals measured for these samples show that rock luminescence dating can potentially extend the dateable age range beyond radiocarbon to allow us to date palaeoenvironmental changes in Marine Isotope Stage 5; this is important for understanding sea ice extent and ice-sheet contributions

to sea-level rise during the last interglacial period.

CRediT authorship contribution statement

Rachel K. Smedley: Writing – review & editing, Writing – original draft, Resources, Project administration, Methodology, Investigation, Formal analysis, Data curation, Conceptualization. **David Small:** Writing – review & editing, Writing – original draft, Resources, Project administration, Methodology, Investigation, Formal analysis, Data curation, Conceptualization. **Erin L. McClymont:** Writing – review & editing, Writing – original draft, Resources, Investigation, Funding acquisition, Conceptualization. **Michael J. Bentley:** Writing – review & editing, Writing – original draft, Resources, Investigation, Funding acquisition. **Dominic A. Hodgson:** Writing – review & editing, Writing – original draft, Resources, Investigation, Funding acquisition. **Alice Graham:** Methodology, Data curation.

Declaration of competing interest

The authors declare that they have no known competing financial interests or personal relationships that could have appeared to influence the work reported in this paper.

Acknowledgments

This work has received funding from the European Research Council (ERC) under the European Union's Horizon 2020 research and innovation programme (grant agreement no. 864637, "ANTSIE"), from the Leverhulme Trust (Research Leadership Award, ELM), and from NERC Grant NE/K003674/1 (MB and DH). DS is supported by Natural Environmental Research Council Independent Research Fellowship NE/T011963/1. Dr Valerie Olive is thanked for the ICP-MS analysis. We thank Neil Tunstall for assistance with handheld pXRF analysis, Eleanor Maedhbh Honan, Stephanie Prince and Henri Robert for sample collection at Utsteinen nunatak, and Andy Hein and Al Davies for help with sampling at Reicheltnevet, Torsviktoppen and Maro Cliffs.

Appendix A. Supplementary data

Supplementary data to this article can be found online at https://doi.org/10.1016/j.quageo.2026.101746.

Data availability

Data will be made available on request.

References

Ageby, L., Angelucci, D.E., Brill, D., Carrer, F., Brüker, H., Klasen, N., 2022. Dating dry-stone walls with rock surface luminescence: a case study from the Italian alps. J. Archaeol. Sci. 144, 105625.

Aitken, M.J., 1985. Thermoluminescence dating: past progress and future trends. Nucl. Tracks Radiat. Meas. 10, 3–6.

Balco, G., Brown, N., Nichols, K., Venturelli, R.A., Adams, J., Braddock, S., Campbell, S., Goehring, B., Johnson, J.S., Rood, D.H., Wilcken, K., Hall, B., Woodward, J., 2023. Reversible ice sheet thinning in the Amundsen Sea embayment during the late Holocene. Cryosphere 17, 1787–1801. https://doi.org/10.5194/tc-17-1787-2023.

Balescu, S., Lamothe, M., 1993. Thermoluminescence dating of the Holsteinian marine formation of herzeele, northern France. J. Quat. Sci. 8, 117–124.

Berg, S., Melles, M., Hermichen, W.-D., McClymont, E.L., Bentley, M.J., Hodgson, D.A., Kuhn, G., 2019. Evaluation of mumiyo deposits from east Antarctica as archives for the late Quaternary environmental and climatic history. G-cubed 20, 260–276.

Björck, V., Malmer, N., Hjort, C., Sandgren, P., Ingolfsson, O., Wallen, B., Smith, R.I.L., Jonsson, B.L., 1991. Stratigraphic and paleoclimatic studies of a 5500-Year-Old moss bank on elephant island, Antarctica. Arct. Alp. Res. 23, 361–374.

Buylaert, J.-P., Jain, M., Murray, A.S., Thomsen, K.J., Thiel, C., Sohbati, R., 2012. A robust feldspar luminescence dating method for middle and late Pleistocene sediments. Boreas 41, 435–451.

Chase, B.M., Meadows, M.E., Scott, L., Thomas, D.S.G., Marais, E., Sealy, J., Reimer, P.J., 2009. A record of rapid Holocene climate change preserved in hyrax middens from Southwestern Africa. Geology 37, 703–706.

Chase, B.M., Scott, L., Meadows, M.E., Gil-Romera, G., Boom, A., Carr, A.S., Reimer, P.J., Truc, L., Valsecchi, V., Quick, L.J., 2012. Rock hyrax middens: a palaeoenvironmental archive for southern African drylands. Quat. Sci. Rev. 56, 107–125.

Colarossi, D., Duller, G.A.T., Roberts, H.M., Tooth, S., Lyons, R., 2015. Comparison of paired quartz OSL and feldspar post-IR IRSL dose distributions in poorly bleached fluvial sediments from South Africa. Quat. Geochronol. 30, 233–238.

Deer, W.A., Howie, R.A., Zussman, J., 2013. An introduction to rock-forming minerals. Mineralogical Society of Great Britain and Ireland. Third edition, Hertfordshire, UK.

Delmonte, B., Petit, J., Maggi, V., 2002. Glacial to Holocene implications of the new 27000-year dust record from the EPICA dome C (east Antarctica) ice core. Clim. Dyn. 18, 647–660.

Elkadi, J., King, G.E., Lehmann, B., Herman, F., 2021. Reducing variability in OSL rock surface dating profiles. Quat. Geochronol. 64, 101169.

Elkadi, J., Lehmann, B., King, G., Steinemann, O., Ivy-Ochs, S., Christl, M., Herman, F., 2022. Quantification of post-glacier bedrock surface erosion in the european alps using ^{10}Be and optically stimulated luminescence exposure dating. Earth Surf. Dyn. 10, 909–928. https://doi.org/10.5194/esurf-10-909-2022.

Freiesleben, T., Sohbati, R., Murray, A.S., Jain, M., al Khasawneh, S., Hvidt, S., Jakobsen, B., 2015. Mathematical Model Quantifies Multiple Daylight Exposure and Burial Events for Rock Surfaces Using Luminescence Dating, vol. 81, pp. 16–22.

Freiesleben, T., Thomsen, K.J., Sellwood, E., Liu, J., Murray, A.S., 2023. Testing new kinetic models and calibration methods for rock surface luminescence exposure dating using controlled experiments. Radiat. Meas. 169, 107033.

Fuhrmann, S., Meyer, M.C., Gliganic, L.A., Obleitner, F., 2022. Testing the effects of aspect and total insolation on luminescence depth profiles for rock surface exposure dating. Radiat. Meas. 153, 106732.

Grieman, M.M., Nehrbass-Ahles, C., Hoffmann, H.M., Bauska, T.K., King, A.C.F., Mulvaney, R., Rhodes, R.H., Rowell, I.F., Thomas, E.R., Wolff, E.W., 2024. Abrupt Holocene ice loss due to thinning and ungrounding in the Weddell Sea embayment. Nat. Geosci. 17, 227–232.

Hajdas, I., Ascough, P., Garnett, M.H., Fallon, S.J., Pearson, C.L., Quarta, G., Spalding, K. L., Yamaguchi, H., Yoneda, M., 2021. Radiocarbon dating 1. https://doi.org/10.1038/s43586-021-00058-7.

Heaton, T.J., 2021. Community comment on "Summer sea-ice variability on the Antarctic margin during the last glacial period reconstructed from snow petrel (Pagodroma nivea) stomach-oil deposits". Clim. Past Discuss. https://doi.org/10.5194/cp-2021-134-CC1.

Heaton, T.J., Blaauw, M., Blackwell, P.G., Bronk Ramsey, C., Reimer, P.J., Marian Scott, E., 2020. The IntCal20 approach to radiocarbon calibration curve construction: a new methodology using Bayesian splines and errors-in-variables. Radiocarbon 62, 821–863.

Heaton, T.J., Butzin, M., Bard, E., Bronk Ramsey, C., Hughen, K.A., Kohler, P., Reimer, P. J., 2023. Marine radiocarbon calibration in polar regions: a simple approximate approach using MARINE20. Radiocarbon 65, 848–875.

Hijmans, R.J., 2019. Raster: geographic data analysis and modeling. R package version 2, 9–23. https://CRAN.R-project.org/package=raster.

Hiller, A., Wand, U., Kampf, H., Stackebrandt, W., 1988. Occupation of the antarctic continent by petrels during the past 35 000 years: inferences from a ^{14}C Study of Ssomach Ois Deposios. dolar Biology 9, 69–77.

Huntley, D.J., Lamothe, M., 2001. Ubiquity of Anomalous Fading in K-feldspars and the Measurement and Correction for It in Optical Dating, vol. 38, pp. 1093–1106.

Jenkins, G.T.H., Duller, G.A.T., Roberts, H.M.R., Chiverrell, R.C., Glasser, N.F., 2018. A new approach for luminescence dating glaciofluvial deposits - high precision optical dating of cobbles. Quat. Sci. Rev. 192, 263–273.

Laskaris, N., Liritzis, I., 2011. A new mathematical approximation of sunlight penetrations in rocks for surface luminescence dating. J. Lumin. 131, 1874–1884.

Lehmann, B., Valla, P.G., King, G.E., Herman, F., 2018. Investigation of OSL surface exposure dating to reconstruct post-LIA glacier fluctuations in the French Alps (Mer de Glace, Mont Blanc massif). Quat. Geochronol. 44, 63–74.

Li, B., Li, S.-H., 2011. Luminescence dating of K-feldspar from sediments: a protocol without anomalous fading correction. Quat. Geochronol. 6, 468–479.

Liu, J., Murray, A., Sohbati, R., Jain, M., 2016. The effect of test dose and first IR stimulation temperature on post-IR IRSL measurements of rock slices. Geochronometria 43, 179–187.

Luo, M., Chen, J., Liu, J., Qin, J., Owen, L., Han, F., Yang, H., Wang, H., Zhang, B., Yin, J., Li, Y., 2018. A test of rock surface luminescence dating using glaciofluvial boulders from the Chinese Pamir. Radiat. Meas. 120, 290–297.

McCarthy, L., Head, L., Quade, J., 1996. Holocene palaeoecology of the northern flinders ranges, South Australia, based on stick-nest rat (leporillus spp.) middens: a preliminary overview. Palaeogeogr. Palaeoclimatol. Palaeoecol. 123, 205–218.

McClymont, E.L., Bentley, M.J., Hodgson, D.A., Spencer-Jones, C.L., Wardley, T., West, M.D., Croudace, I.W., Berg, S., Gröcke, D.R., Kuhn, G., Jamieson, S.S.R., Sime, L., Phillips, R.A., 2022a. Summer sea-ice variability on the antarctic margin during the last glacial period reconstructed from snow petrel (Pagodroma nivea) stomach-oil deposits. Clim. Past 18, 381–403. https://doi.org/10.5194/cp-18-381-2022.

McClymont, E.L., Bentley, M.J., Hodgson, D.A., Spencer-Jones, C.L., Wardley, T., West, M.D., Croudace, I.W., Berg, S., Grocke, G., Kuhn, G., Jamieson, S.S.R., Sime, L. C., Phillips, R.A., 2022b. Snow petrel stomach-oil deposits as a new biological archive of antarctic sea ice. Past Global Changes Magazine 30 (2), 82–83.

McClymont, E.L. et al. (Submitted) Seabird Population Changes Driven by Antarctic Ice Sheet and sea-ice Extent.

Meyer, M.C., Gliganic, L.A., Jain, M., Schmidmair, D., 2018. Lithological controls on light penetration into rock surfaces – implications for OSL and IRSL surface exposure dating. Radiat. Meas. 120, 298–304.

Mulvaney, R., Abram, N.J., Hindmarsh, R., Arrowsmith, C., Fleet, C., Triest, J., Sime, L. C., Alemany, O., Foord, S., 2012. Recent antarctic peninsula warming relative to Holocene climate and ice-shelf history. Nature 489, 141–144.
Murray, A.S., Thomsen, K.J., Masuda, N., Buylaert, J.-P., Jain, M., 2012. Identifying well-bleached quartz using the different bleaching rates of quartz and feldspar luminescence signals. Radiat. Meas. 47, 688–695.
Murray, A.S., Buylaert, J.-P., Guerin, G., Qin, J., Singhvi, A.K., Smedley, R.K., Thomsen, K.T., 2021. Optically stimulated luminescence dating using quartz sand. Nat. Rev. Methods Primers 1, 72.
Ou, X.J., Roberts, H.M., Duller, G.A.T., Gunn, M.D., Perkins, W.T., 2018. Attenuation of light in different rock types and implications for rock surface luminescence dating. Radiat. Meas. 120, 305–311.
Ou, X.J., Roberts, H.M., Duller, G.A.T., 2022. Rapid assessment of beta dose variation inside cobbles, and implications for rock luminescence dating. Quat. Geochronol. 72, 101349.
Penny, C.E., 2025. Past sea-ice and Ice Sheet Configurations in the Eastern Weddell Sea. Durham University. PhD Thesis.
Prescott, J.R., Hutton, J.T., 1994. Cosmic ray and gamma ray dosimetry for TL and ESR. Nucl. Tracks Radiat. Meas. 14, 223–227.
Riedesel, S., Autzen, M., 2020. Beta and gamma dose rate attenuation in rocks and sediment. Radiat. Meas. 133, 106295.
Robins, R., Robins, A., 2011. The antics of ants: ants as agents of bioturbation in a midden deposit in south-east Queensland. Environ. Archaeol. 16, 151–161.
Simms, A.R., DeWitt, R., Kouremenos, P., Drewry, A.M., 2011. A new approach to reconstructing sea levels in Antarctica using optically stimulated luminescence of cobble surfaces. Quat. Geochronol. 6, 50–60.
Small, D., Fulop, R., Smedley, R.K., Lees, T., Trabucatti, S., Fabel, D., Miguens-Rodriguez, M., Boeckmann, G., 2025. A thinner-than-present west antarctic ice sheet in the southern Weddell Sea embayment during the Holocene. EGUsphere. https://doi.org/10.5194/egusphere-2025-4794 (preprint).
Smedley, R.K., 2018. Dust, sand and rocks as windows into the past. Elements 14, 9–14.
Smedley, R.K., Duller, G.A.T., Pearce, N.J.G., Roberts, H.M., 2012. Determining the K-content of single grains of K-feldspar for luminescence dating. Radiat. Meas. 47, 790–796.
Smedley, R.K., Duller, G.A.T., Roberts, H.M., 2015. Assessing the bleaching potential of the post-IR IRSL signal for individual K-feldspar grains: implications for single-grain dating. Radiat. Meas. 79, 33–42.
Smedley, R.K., Pearce, N.J.G., 2016. Internal U and Th concentrations of K-feldspar grains: implications for luminescence dating. Quat. Geochronol. 35, 16–25.
Smedley, R.K., Small, D., Jones, R.S., Brough, S., Bradley, J., Jenkins, G.T.H., 2021. Erosion rates in a wet, temperate climate derived from rock luminescence techniques. Geochronology 2021, 1–26. https://doi.org/10.5194/gchron-3-525-2021.
Sohbati, R., Murray, A.S., Jain, M., Buylaert, J.P., Thomsen, K.J., 2011. Investigating the resetting of OSL signals in rock surfaces. Geochronometria 38, 249–258.
Stevenson, M.A., Hodgson, D.A., Bentley, M.J., Grocke, D.R., Tunstall, N., Longley, C., Graham, A., McClymont, E.L., 2025. Mid-holocene sea-ice dynamics and climate in the northeastern Weddell Sea inferred from an antarctic snow petrel stomach oil deposit. Clim. Past 21, 2465–2483.
Suganuma, Y., Kaneda, H., Mas e Braga, M., Ishiwa, T., Koyama, T., Newall, J.C., Okuno, J., Obase, T., Saito, F., Rogozhina, I., Andersen, J.L., Kawamata, M., Hirabayashi, M., Lifton, N.A., Fredin, O., Harbor, J.M., Stroeven, A.P., Abe-Ouchi, A., 2022. Regional sea-level highstand triggered Holocene ice sheet thinning across coastal dronning maud land, east Antarctica. Commun. Earth Environ. 3, 273. https://doi.org/10.1038/s43247-022-00599-z.
Theilen, B.M., Simms, A.R., DeWitt, R., Zurbuchen, J., Garcia, C., Gernant, C., 2023. The impact of the neoglacial and other environmental changes on the raised beaches of joinville island, Antarctica. Antarct. Sci. 35, 418–437.
Thomsen, K.J., Murray, A.S., Jain, M., Bøtter-Jensen, L., 2008. Laboratory fading rates of various luminescence signals from feldspar-rich sediment extracts. Radiat. Meas. 43, 1474–1486.
Thomsen, K.J., Kook, M., Murray, A.S., Jain, M., 2018. Resolving luminescence in spatial and compositional domains. Radiat. Meas. 15, 260–266.
Verleyen, E., Hodgson, D.A., Sabbe, K., Cremer, H., Emslie, S.D., Gibson, J., Hall, B., Imura, S., Kudoh, S., Marshall, G.J., McMinn, A., Melles, M., Newman, L., Roberts, D., Roberts, S.J., Singh, S.M., Sterken, M., Tavernier, I., Verkulich, S., Van de Vyver, E., Van Nieuwenhuyze, W., Wagner, B., Vyverman, W., 2011. Post-glacial regional climate variability along the east antarctic coastal margin—Evidence from shallow marine and coastal terrestrial records. Earth Sci. Rev. 104, 199–212.
Wintle, A.G., 1973. Anomalous fading of thermo-luminescence in mineral samples. Nature 245, 143–144.
Wurz, S., Pickering, R., Mentzer, S.M., 2022. U-Th dating, taphonomy, and taxonomy of shell middens at klasies river main site indicate stable and systematic coastal exploitation by MIS 5c-d. Front. Earth Sci. 10. https://doi.org/10.3389/feart.2022.1001370.
Zazula, G.D., Froese, D.G., Elias, S.A., Kuzmina, S., Mathewes, R.W., 2007. Arctic ground squirrels of the mammoth-steppe: paleoecology of late Pleistocene middens (~24 000–29 450 14C yr BP), Yukon territory, Canada. Quat. Sci. Rev. 26, 979–1003.